Numerical Simulation of Forced Convective Heat Transfer Coefficients on Shaded Roofs with Wind Circulation in Low-Rise Buildings
การจำลองเชิงตัวเลขเพื่อหาค่าสัมประสิทธิ์การพาความร้อนแบบบังคับภายใต้กระแสลมหมุนบนหลังคาอาคารเตี้ยที่มีอุปกรณ์บังแดด

Sudaporn Chungloo
สุดาภรณ์ ฉุ้งลู้

Faculty of Architecture and Planning, Thammasat University, Pathumthani 12121, Thailand
คณะสถาปัตยกรรมศาสตร์และการผังเมือง มหาวิทยาลัยธรรมศาสตร์ จังหวัดปทุมธานี 12121
E-mail: chungloo@tu.ac.th

Abstract

The convective heat transfer coefficient at the external wall of the building is an important variable in the calculation of heat transfer through the building envelope. The average value of this variable has been estimated from the empirical equation of the wind speed around the building. This research used computational fluid dynamics program (CFD), Phoenics 3.5, to compute the convective heat transfer coefficients as the shading device is fixed on the roof regarding the wind separation and recirculation around the building. The results of the coefficient of convective heat transfer derived from modeling a building with no shading device were compared with the experimental results in previous research works. The simulation results were validated in the simulated model with turbulent flow using Large Eddy Simulation (LES). After that, the model with LES approach known as the standard Smagorinsky model (SMG) was applied to the building models with shading device on the roof. The results of this research are the convection coefficient values at the roof surface for a 1.8 meter channel between the roof and shading device and a roof in the wind direction with a length of 8.0, 20.0 and 36.0 meters, representing a 2-storey house and 4-storey buildings. The derived coefficients are proposed as power-law functions of fixed points on the roof and shading device surfaces. The highest convective heat transfer is predicted at the sharp upstream edge, two span-wise rims for the 4-storey building and most of the area of the 2-storey house. Installing eaves or placing buffer zones around the top floor of building is recommended in addition to the shading device on the roof.

บทคัดย่อ

ค่าสัมประสิทธิ์การพาความร้อนที่ผนังด้านนอกอาคารเป็นตัวแปรสำคัญตัวแปรหนึ่งในการคำนวณการถ่ายเทความร้อนผ่านกรอบอาคาร โดยทั่วไปค่าเฉลี่ยของตัวแปรดังกล่าวสำหรับกรอบอาคารสามารถประมาณได้จากสมการเชิงประจักษ์ของความเร็วลมภายนอกรอบอาคาร งานวิจัยนี้ใช้โปรแกรมคำนวณพลศาสตร์ของไหล Phoenics 3.5 คำนวณค่าสัมประสิทธิ์การพาความร้อน เมื่อคำนึงถึงกระแสลมที่ชนกับอาคารแล้วแยกตัวออกและเกิดการหมุนรอบอาคาร โดยเฉพาะกรณีที่มีการใช้งานอุปกรณ์บังแดดชนิดถาวรบนหลังคาอาคาร ผลของค่าสัมประสิทธิ์การพาความร้อนจากแบบจำลองอาคารที่ไม่มีอุปกรณ์

บังแดดเปรียบเทียบกับผลจากการทดลองในงานวิจัยก่อนหน้า พบว่า มีความใกล้เคียงกันเมื่อจำลองการไหลแบบปั่นป่วนโดยวิธี Large Eddy Simulation (LES) ที่ขึ้นอยู่กับเวลา วิธีจำลอง LES ด้วยแบบจำลอง Smagorinsky มาตรฐาน ถูกนำไปใช้ต่อในการจำลองหลังคาอาคารที่ติดตั้งอุปกรณ์บังแดดที่หลังคา ผลสรุปของงานวิจัย ได้แก่ ค่าสัมประสิทธิ์การพาความร้อนที่ตำแหน่งต่าง ๆ ของหลังคาอาคารโดยมีระยะห่างระหว่างอุปกรณ์บังแดดกับหลังคาที่ 1.8 เมตร ความยาวของหลังคาในทิศการไหลของลมระหว่าง 6.0 20 และ 36 เมตร ซึ่งแทนหลังคาบ้านพักอาศัยสองชั้นและอาคารตึกแถว 4 ชั้น ผลของค่าสัมประสิทธิ์ที่ได้จากการจำลองนำเสนอด้วยความสัมพันธ์แบบยกกำลังของความเร็วลมที่จุดใด ๆ บนผิวหลังคาและผิวอุปกรณ์บังแดด การศึกษาพบว่า ค่าสัมประสิทธิ์การพาความร้อนมากที่สุด ซึ่งหมายถึงการพาความร้อนและการถ่ายเทความชื้นสูงที่สุดอยู่ที่ขอบหลังคาด้านต้นลม ขอบด้านข้างของหลังคาและอุปกรณ์บังแดดในกรณีอาคาร 4 ชั้น และพบค่าสูงสุดที่ขอบและบนพื้นระนาบส่วนใหญ่ของหลังคาบ้านพักอาศัยสองชั้น จึงมีข้อแนะนำให้ชั้นบนสุดมีชายคายื่นหรือมีพื้นที่กันชนกับสภาวะภายนอกเพิ่มเติมจากการใช้อุปกรณ์บังแดดให้กับหลังคา

Keywords

Computational Fluid Dynamics (การคำนวณพลศาสตร์ของไหล)
Building Envelope (กรอบอาคาร)
Shading Roof (หลังคาบังแดด)
Natural Wind Ventilation (การระบายอากาศโดยลมธรรมชาติ)
Forced Convective Heat Transfer Coefficient (สัมประสิทธิ์การพาความร้อนแบบบังคับ)

1. Introduction

Information on convective heat transfer coefficient (h_c) on the exterior wall is important for the investigation of heat, air and moisture transport at the building facade. Typically, the average value of h_c (W/m^{2}K) is applied in calculation as follows:

$$h_c = q_{conv}/(T_s - T_{ref}) \quad [1]$$

where q_{conv} is the convective heat flux (W/m^2), T_s is the surface temperature (K) and T_{ref} is the reference temperature (K) and can be the ambient temperature outside the boundary layer. From equation [1], h_c can be viewed as the ratio between the actual convective heat transfer and the difference T_s - T_{ref}, where the actual amount of convective heat transfer is governed by the characteristic of flow adjacent to the surface, called the boundary layer. For example, a laminar or a turbulence flow over the surface varies the local h_c and the amount of convective heat transfer distinctively. It has been clearly shown that the h_c is the function of wind velocity (Blocken, Defraeye, Derome & Carmeliet, 2009; Givoni, 1994). In a large area like a building facade, local h_c should be used instead of the average value of h_c since flow characteristics over the entire surface are diverse. The application of h_c is also found in the thermal performance of single and double-skin facades, green houses, solar chimney, photovoltaic arrays and wetting and drying of large scale urban climatology. In addition, analysis of moisture transport through the building facade requires the knowledge of convective moisture transfer coefficient that is also calculated in a similar way to h_c (Blocken et al., 2009).

The previous researches on determining $h_c$were experiments of small scale in wind tunnel, full scale measurement and calculation by computational fluid dynamic program (CFD). The external flow of fluid around an opaque object has been known as bluff body aerodynamics where the flow patterns can be visualized using smoke injection and an oil tray (Meinders, Van der Meer & Hanjali, 1998). To investigate details of velocity structure, average and local h_c, a sophisticated instrument like an infrared camera and Laser Doppler Anemometer (LDA) were applied (Meinders & Hanjali, 1999). The experiment on flow patterns around a matrix of cubes at a high Reynolds (*Re*) number by Meinders & Hanjalic (1999) has been recognized as the validated results of several computational researches (Cheng, Lien, Yee & Sinclair 2003; Heminda, Spehr & Krajnovic, 2008; Blocken, Defraeye, Derome & Carmeliet, 2009). The experiments were carried out on the 15 x 15 x 15 mm^3 cubes representing the electronic components attached to the printed circuit where the ventilation was required to prevent the technical failure. The Reynolds number based on the cube's height and the mean bulk velocity were 2,851-5,280 and no effect was found on the value of local h_c scaled by average h_c. The regions of flow around the bluff body based on the experiment of Meinders are 1) the horseshoe type of vortex at the windward face wrapping around the side walls, 2) the arc-shaped vortex in the wake, 3) the separation bubbles on the rooftop and the side walls originating from the windward edges, and 4) downwash of the flow as shown in Figure 1. Figure 1 also shows the oil visualization of the horseshoe vortex shape in the cube matrix.

Covering the roof of a building with shading, i.e. double roofs, has been suggested for building design in hot and humid climates. The main function of the additional shading device is to prevent direct sunlight during the day time, provide wind ventilation between the roof and the shading, and let the collected heat dissipate to the sky during the night time. Among the field measurement (Hagishima & Tanimoto, 2003) and computational studies of bare roofs and facades, flow characteristics and the h_c of the roof with shading devices have been rarely investigated. Therefore, this research focuses on determining the values of hc for low rise buildings of 8m x 8m x 6m, 36m x 20m x 14m, and 20m x

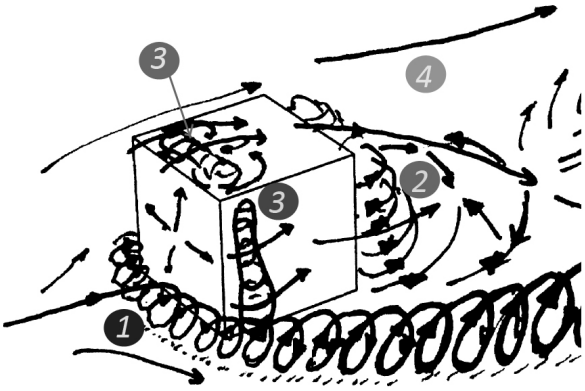

(a)

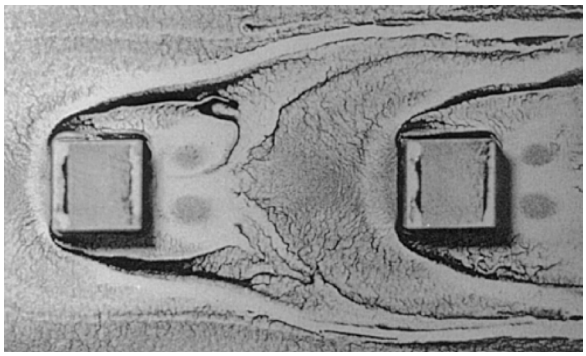

(b)

Source: Meinders & Hanjali, 1999

Figure 1. a) Flow patterns around a cube, consisting of (1) the horseshoe type of vortex, (2) the arc-shaped vortex in the wake, (3) the separation bubbles on the rooftop and the side walls, and (4) downwash of the flow; and b) oil visualization of flow.

36m x14m (width x depth in the wind direction x height) installed with a fixed shading. The provided dimensions represent typical buildings such as a 2-storey house and a low-rise townhome in Thailand. Taking into account the flow characteristics around the building, wind velocity of 1, 2, 3 and 4 m/s under a temperature differences (T_s-T_{ref}) of 6.0°C are studied.

2. Numerical Models

Computer programs have been developed and applied to simulate complex flow. The most widely used approach in modeling flow is the average Reynolds-averaged Navier-Stokes (RANS) method, including the k-ε model. However, this approach is less accurate and certain for a large scale computation, such as flows around building-like obstacles, compared to the Large Eddy Simulation (LES) method (Rodi, 1997). The k-ε model over-predicts the separation length by 35-110%, while the LES method using standard Smagorinsky model (SMG) over-predicts it by 7%. In LES, the standard Smagorinsky has been widely used on account of its computational simplicity and numerical stability (Cheng, Lien, Yee & Sinclair, 2003). Computation using the LES method is costly since an expensive computer is usually needed to cope with the time consuming process of the simulation.

In addition to the selection of a good and appropriate methodology in the simulation of bluff body, studying h_c associates with an accurate near-wall modeling technique. There are two options usually used in CFD modeling, the low-Reynolds number modeling and wall functions. The low-Reynolds number means resolving all cells at the near-wall boundary layer where it needs a large number of fine grinds that bring a high computational cost. The wall function can solve the coarse near-wall grids since the function approximates the effect of the wall on the mean wind speed, turbulence quantities and temperature in the layer known as law-of-the-wall. The standard and non equilibrium wall function is valid for the 2D flow with small pressure gradient, but not with the complex 3D flow involving impingement, separation, and reattachment such as flow around buildings. For a windward facade, the low-Reynolds number modeling under steady state was suggested for computing h_c on the windward facade and LES or DES (Detached Eddy Simulation) were recommended for other facades of a building (Blocken et al., 2009). As the flow and h_c on the roof (top facade) is considered in this study, the LES method is chosen and the near-wall grids are high in resolution. The governing equation of LES and k-ε models can be found in the literatures (Cheng et al, 2003; Versteeg & Malalasekra, 1995).

The simulation results in this paper are composed of two parts: 1) validation with previous

researches where buildings contain no shadings and 2) results of h_c obtained from LES approach involving buildings with shadings on roofs. In the first part, a building of 10m x 10m x 10m was simulated using k-ε model, low-Reynolds number model, and Standard SMG model, and the results compared for top and windward facades. The derived simulation results of flow characteristics around buildings are also compared with the experimental results of Meinders & Hanjali (1999). In the second part, low-rise buildings are a 2-storey house and a 4-storey row building with flat shading device at 1.8 m above their roofs. The objectives are to determine the distribution of the h_c across the roof and on its shading device, to analyze the variation of the h_c with wind speed, and to analyze the relationship between h_c and wind velocity at the roof surface.

3. Numerical Model Set Up

3.1 Building Models and Computational Grids

Hexahedral non-uniform grids are used in all models. The high resolution grids were applied near the building walls and at the ground to capture the development of the flow near the wall surfaces. The building shapes, grids, and wind direction are shown in Figure 2. The Phoenics 3.5 commercial package is used to generate these cells. The two models 3A and 3B are similar but the wind direction strikes the 36 x 14 m^2 facade in Model #3A and the 24 x 14 m^2 facade in Model #3B. The domain size, smallest grid size, total number of cells, turbulence models, differencing schemes and times spend in running models# 1, 2, 3A and 3B are shown in Table1. In all models, x is the direction of the wind. The hybrid differencing scheme in Phoenics program is the central-differencing scheme. This validated with previous work that used the low Reynolds model, hence Model #1 was simulated using steady low Reynolds model. The k-ε model, as a widely used model in engineering studies and the simulation industry, was simulated to compare their results with

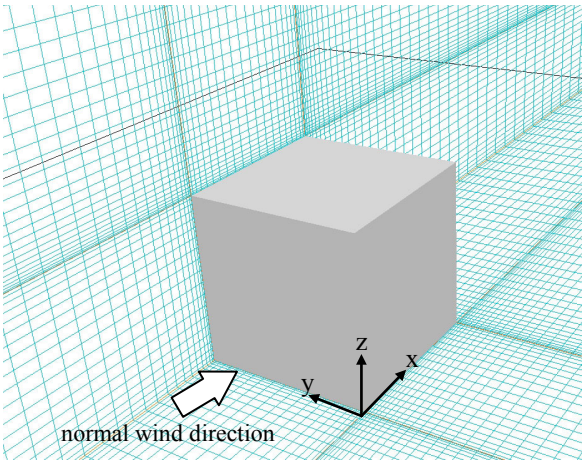

(a)

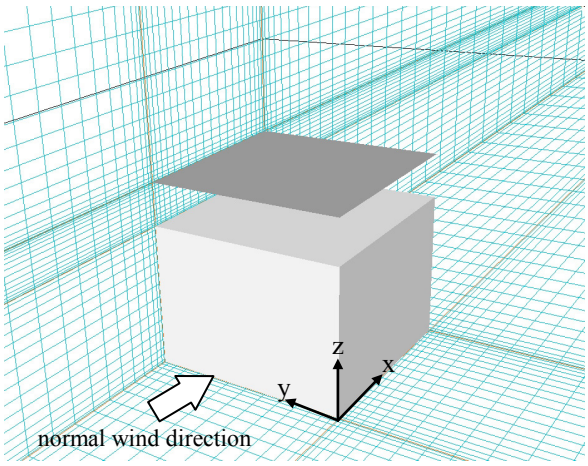

(b)

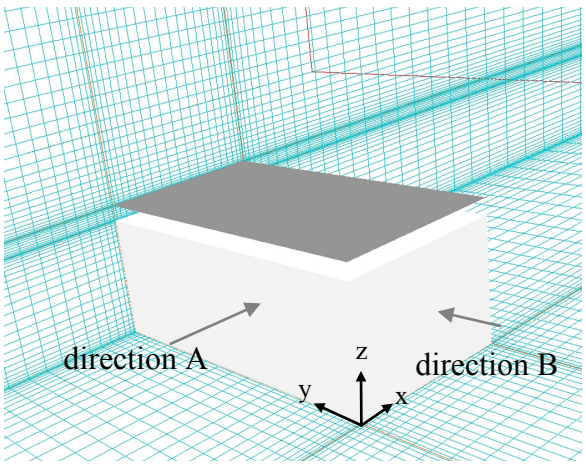

(c)

Figure 2. a) Model #1: 10m x 10m x 10m building for validation, b) Model #2: 8m x 8m x 6m with shading, c) Model #3A 36m x 20m x 14m (wind direction A), and Model #3B 20m x 36m x 14m with shading (wind direction B)

Table 1. Geometric and numerical inputs and total time used in simulation.

Input	Model #1	Model #2	Model #3A	Model #3B
Domain size (x, y, z)	120, 80, 50	120, 80, 50	240, 252, 60	260, 200, 60
Smallest grid in x, y, z direction (m)	0.025, 0.022, 3.2E-03	0.028, 0.034, 2.7E-03	0.023, 0.028, 8.1E-04	0.019, 0.029, 5.2E-03
Number of grids in domain	349,272 598,000 for LES	335,544	698,560	804,384
Turbulence Model	k-ε (steady) low Reynolds (steady) LES (transient)	LES (transient)	LES (transient)	LES (transient)
Differencing scheme	Hybrid	Hybrid	Hybrid	Hybrid
Near-wall model	General log law for low-Reynolds, log law for others	log law	log law	log law
Time at last step (sec)	600	300	300	300
Iteration/time step	50	50	50	50
Time used for run (hour:min)	4:53 for k-ε 6:28 for low Reynolds 47:20 for LES	12:37	30:00	58.28

those LES and low Reynolds models. The transient LES model was simulated as the most expensive model with acceptable accuracy. An iteration/time step of 50 is recommended by Pheonics (Concentration Heat and Momentum [CHAM], 2010). The PC with CPU Intel Core(TM) i7 at 2.2 GHz in this study determines time spending on simulations. The simulations were terminated as the results did not change significantly, counting for 3,000-5,000 iteration on steady-state models and 260-300 second in transient models.

3.2 Boundary Condition

The thermal boundary conditions for Model #1 are a fixed building surface temperature of 30°C, inlet air temperature of 10°C and the reference temperature to determine h_c is 10°C. The average turbulence intensity was 15% and the mean bulk velocity is 3m/s. Surface and ambient temperatures of Model #2, #3A and #3B are taken from previous experiment of solar chimney test cells (Chungloo, 2007). The surface and ambient temperatures and wind velocity were measured during 6.00 am - 6.30 pm in May-June 2007-2009. The average value of the measured surface and ambient temperatures at 4.30 pm, given the highest surface temperature of the daytime, are applied here. Surface temperatures of roof, shading device on roof, West, South, North, and East walls are 37.2, 42.4, 37.4, 37.0, 36.2, and 36.2°C, respectively. The difference between the wind and wall temperatures is only 1.0-6.2°C in the actual environment. The inlet wind is the wind profile with z = 2.4E-04 and temperature of 35.8°C and the windward facade is the north wall. In all models, walls are assumed to be smooth no-slip surfaces and the bottom of the domain is the adiabatic wall. The simulation results are presented in the next section.

4. Results and Discussions

4.1 CFD Validation

CFD simulation based on RANS equations in combination with a turbulence model require validation, which can be performed by comparison

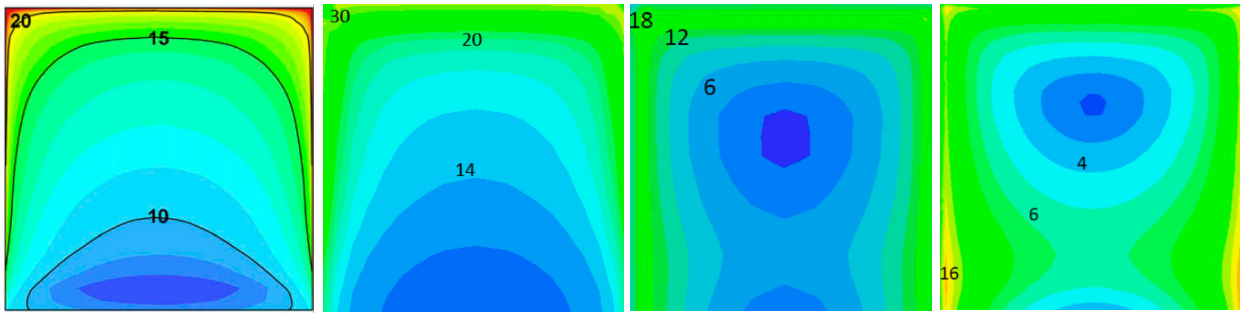

(a) (b) (c) (d)

Figure 3. Results of hc (W/m^{2}K) on the windward facade by applying (a) low Reynolds turbulence models with 1.88 x106 grids in the previous study (Blocken, 2009), (b) low Reynolds turbulence models with 3.5 x105 grids in this study, (c) k-ε model and (d) LES approach.

of the CFD results with either full-scale measurements or wind tunnel data. Prior to the CFD validation with the measurement, the simulation of cube 10 m^3 (Model #1) in this study is compared to the 10 m^3 cube in the previous study of Blocken et al. (2009) for the windward wall as shown in Figure 3. Figure 3 shows that the CFD model applying low Reynolds turbulence model in this study (Figure 3b) gives a result of h_c distribution similar to the previous study (Figure 3a), but those obtained from the steady k-ε and LES approach disagree with previous results. Unlike the low Reynolds model, the k-ε and LES models are not recommended for studying the windward facade.

Due to the lack of available wind-tunnel data of h_c on the top surface of a cube, validation based on the actual measurement of $h_c/h_{c\ avg}$ on the windward and top surface of a 25 mm^3 cube of Meinders & Hanjali (1999) is performed. The results of wind profiles at center plane of the cube applying low Reynolds, k-ε models and LES approach for x-z plane are shown in Figure 4a-4c and x-y plane are shown in Figure 5a-5c. Generally, flow structure such as the downwash and the horseshoe vortex at the front facade were captured reasonably well by all models. Among these models, LES approach with standard SMG was found to give the best conformance with the details of the experimental visualization. For example, the strong circulations at the top surface,

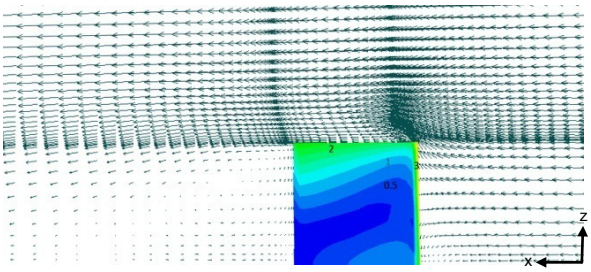

(a) steady low Reynolds

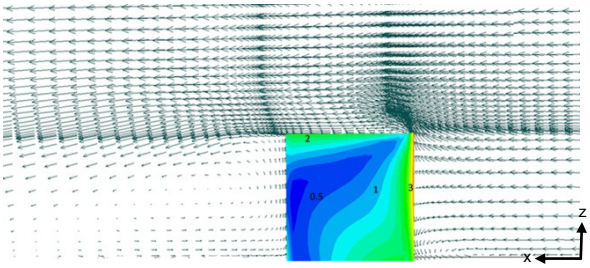

(b) steady k-ε model

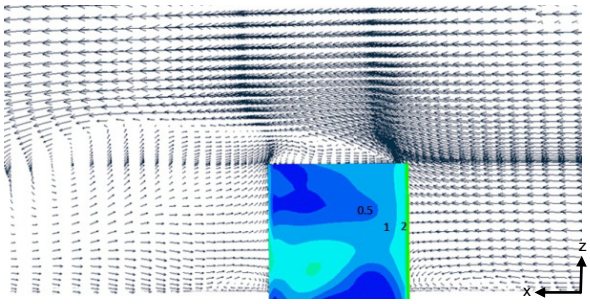

(c) transient LES approach at 260 second

Figure 4. The wind profile in x-z plane with velocity contour (m/s) on the side facade

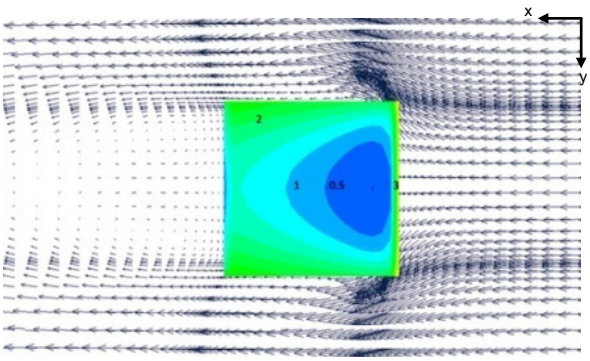

(a) steady low Reynolds model

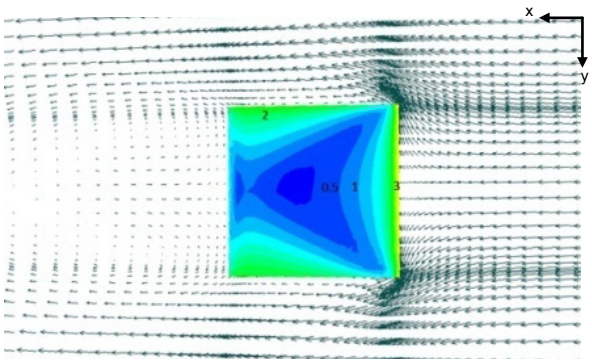

(b) steady k-ε model

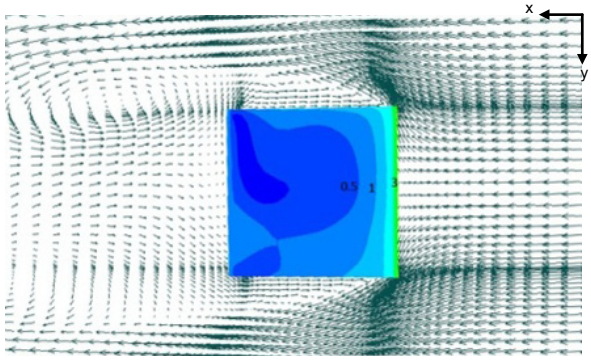

(c) transient LES approach at 260 second

Figure 5. The wind profile in x-y plane with velocity contour (m/s) on the top facade.

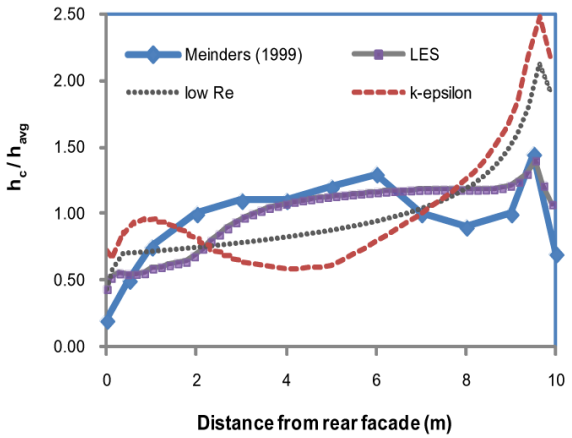

Figure 6. Heat transfer coefficient distribution over the roof surface applying the LES approach, low Reynolds model and k-ε model and experimental results of Meinders & Hanjali (1999).

side walls and the downstream of the building are better captured by LES approach (Figure 4c and 5c). Also, the recirculation of velocity contour on the side wall shows the small separation bubbles occur as depicted in the experiments of Meinders. The top views of the buildings shown in Figure 5c indicate velocity distribution over the surface and the detail within the horseshoe vortex is clearly illustrated. Considering only the top surface, the values of the local heat transfer coefficient (h_c) normalized with the average heat transfer coefficient ($h_{c,\,avg}$) of low Reynolds model, k-ε turbulence models and LES (SMG) approach are compared with the experiment of Meinders & Hanjali (1999) as shown in Figure 6. The lowest value of $h_c/h_{c,\,avg}$ is found at the rear of the top surface where circulation of wind is highest. The recirculation acts as an insulation layer, preventing heat convected from the surface and resulting in minimal h_c. The highest value of h_c in the vicinity of the front edge is due to the reattachment of the shear layer. Therefore, the value of normalized h_c i.e. $h_c/h_{c,\,avg}$, on the top surface of a cube building could be moderately predicted using the LES approach. This approach is used for computing the value of h_c in the study of a building with shaded roof.

4.2 Effect of Shadings on Flow Structure

This section explores the influence of the shading on the velocity and h_c values distribution. Figure 7 displays the instantaneous flow structures around the 8 x 8 x 6 m^3 building projected to the xz-, xy- and yz-planes. The normal wind impinges on the stream-wise face of the building, causing a region with high pressure. The stagnation with high pressure is shown in Figure 7a at $z/H \cong 0.6$ (H = height of the building). Due to the high pressure in the stream-wise face, the flow moves up to strike the shading device and down towards the lateral faces. The flow also directly impinges on the shading device and forms bubbles of circulation and reattachment near the edge. Figure 7b shows two

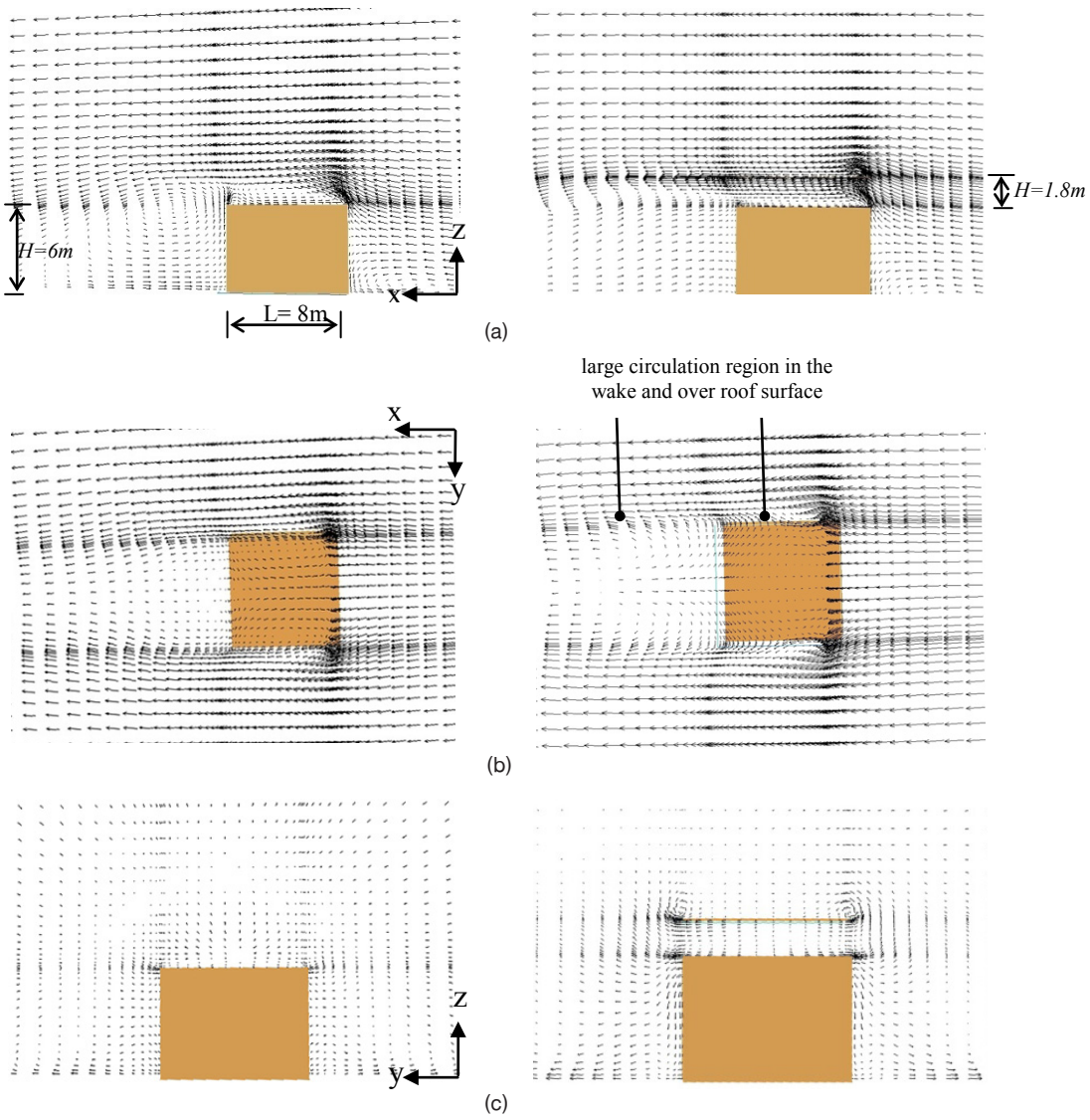

Figure 7. The 8 x 8 x 6 m^3 building without shading device on roof (left column) and with shading device on 1.8 m from the roof surface (right column). Velocity vectors projected to the a) xz-plane at the center of building, b) xy-plane at 0.3 m above the roof, and c) yz-plane at the center of building.

circulation bubbles in the wake flow at the height of the shading (6.3 m from floor). The flow coming from the sides of the building separates from the surface and circulates to form these recirculation bubbles. Figure 7c illustrates the bubbles of reattachment near edges of the roof and the shading device. These reattachments cause high h_c value close to the roof edge as shown in the next section. In addition, the circulation of air under the shading device in Figure 7c indicates low air velocity that would bring low h_c value and convection heat transfer. Compared to the building without shading on the roof, the building with shading device generates one larger circulation region in the channel and larger wakes behind the building (Figure 7b).

The instantaneous flow at 300 sec of a 36 x 20 x 14 m^3 building (Model #3A) is shown in Figure 8a. The stagnation shown in Figure 8a was at $z/H \cong$ 0.8 (H = height of the building). The wind velocity at 14 m from the floor is higher than that at 6 m, hence wind flows through the channel between the roof and shading device without circulation. The reattachment

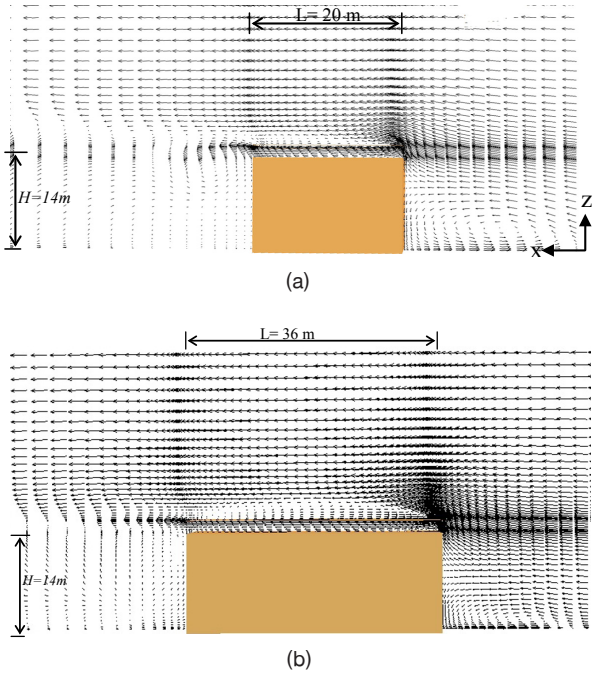

Figure 8. Velocity vectors projected to the (a) xz-plane at the center of 36 x 20 x 14 m^3 and (b) 20 x 36 x 14 m^3 buildings.

and circulation clearly found over the surface of shading device bring about the high h_c value at the edge and reduction of h_c value on the downstream surface of the shading device. The flow structure of Model #3A and #3B are similar except the circulation occurs downstream of the roof in Model #3B in Figure 8b.

4.3 Distribution of h_c Value Across the Roof and Shading Device

The distribution of h_c values across the roof and the shading device, calculated with LES (SMG) model, is displayed in Figure 9 for U_{10} = 2 m/s and for wind direction of 0° with respect to the building. In all models, the h_c value decreases from the upstream edge to the downstream edge of the roof

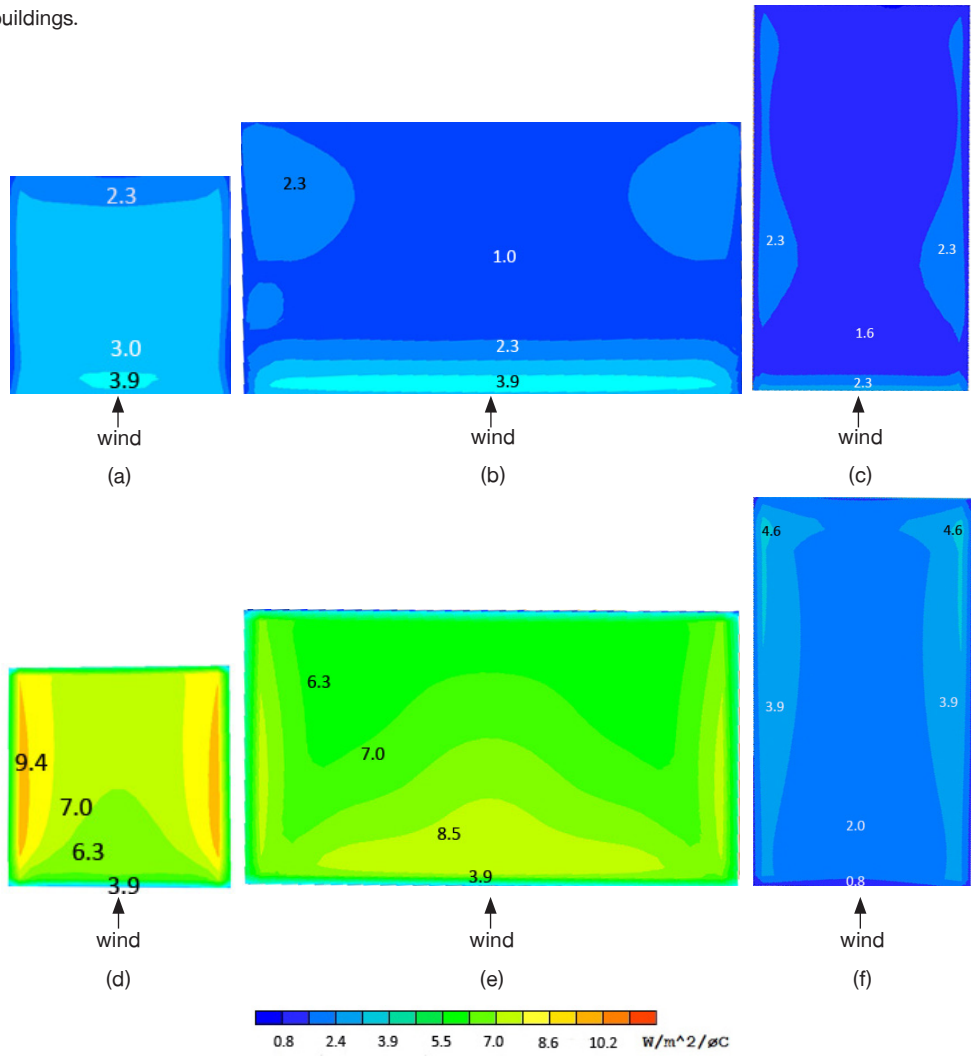

Figure 9. Distribution of hc values across the roof of (a) Model #2, (b) Model #3A, (c) Model #3B and shading device at 1.8 m over the roof of (d) Model #2, (e) Model #3A, (f) Model #3B.

excluding the span-wise rims where flow reattachments take place. The highest values are found close to the edge of the roof and shading device, attributed to the local acceleration at locations that reduce the thickness of the boundary layer. The gradient of h_c values on the shading device is higher than that of the roof. Considering the center region of all building models, the h_c values on the shading device are 2.3, 6.5 and 1.3 times higher than those of the roof in Model #2, Model #3A and Model #3B, respectively.

4.4 Correlation at Fixed Position

At fixed positions on the roof and shading device, the correlation between h_c value and local wind velocity (V_{loc}) can be investigated. Previous researchers showed correlation between h_c and local wind velocity, h_c and the reference wind velocity (U_{10}), and U_{10} and V_{loc} (Blocken et al., 2009; Hagishima & Tanimoto, 2003). A similar analysis is also shown here for specific cases of low rise buildings with shading devices on the roof.

4.4.1 Correlation of U_{10} Value and V_{loc}

Values of V_{loc} at distance 0.3 m above the roof and shading device surfaces are extracted from the simulation results since it was a distance previously measured by Blocken et al. (2009). Results are presented by 8 points in Model #2, 20 points in Model #3A and 14 points in Model #3B as shown in Figure 10. Half of the simulated results are considered because the flow patterns in all building models are symmetrical. Specific positions are denoted by two numbers. For instance, P21 represents the position at the second column (x-axis) and the first row (y-axis).

Figure 11 indicates that at every roof position, there is a different linear correlation between V_{loc} and U_{10}. This corresponds also with the previous research (Blocken, 2009) that the flow around bluff bodies with sharp edges generates a linear relationship between the V_{loc} and U_{10} and this is also true for the other distance d and facade direction. The advantage of correlation between V_{loc} and U_{10} are

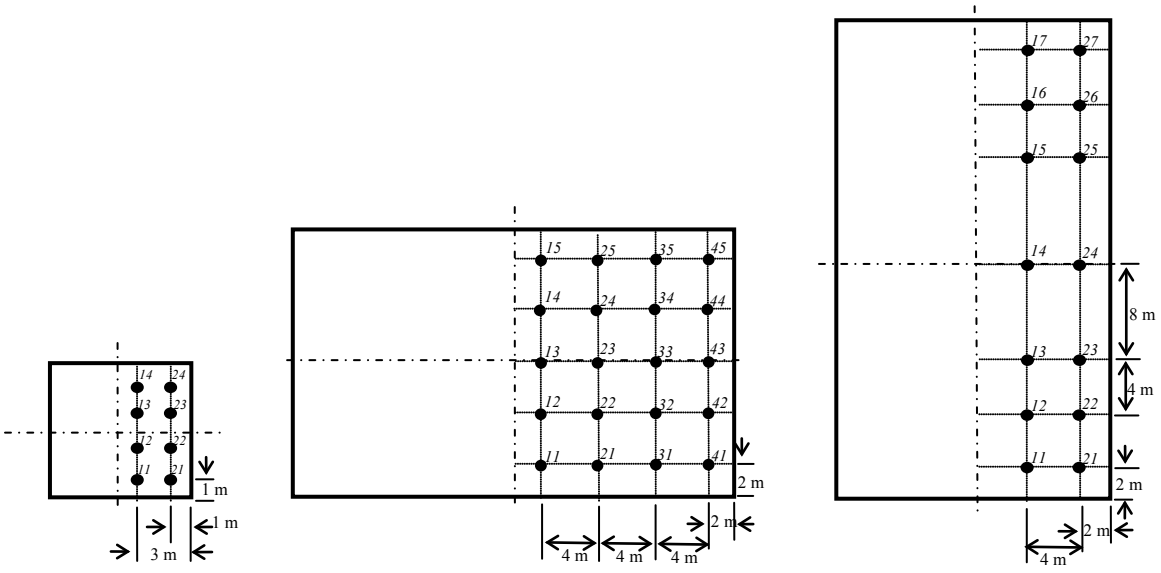

(a) Model #2 (b) Model #3A (c) Model #3B

Figure 10. Points to measure V_{loc} (at distance 0.3 m above surface) and h_c values of roof and shading device.

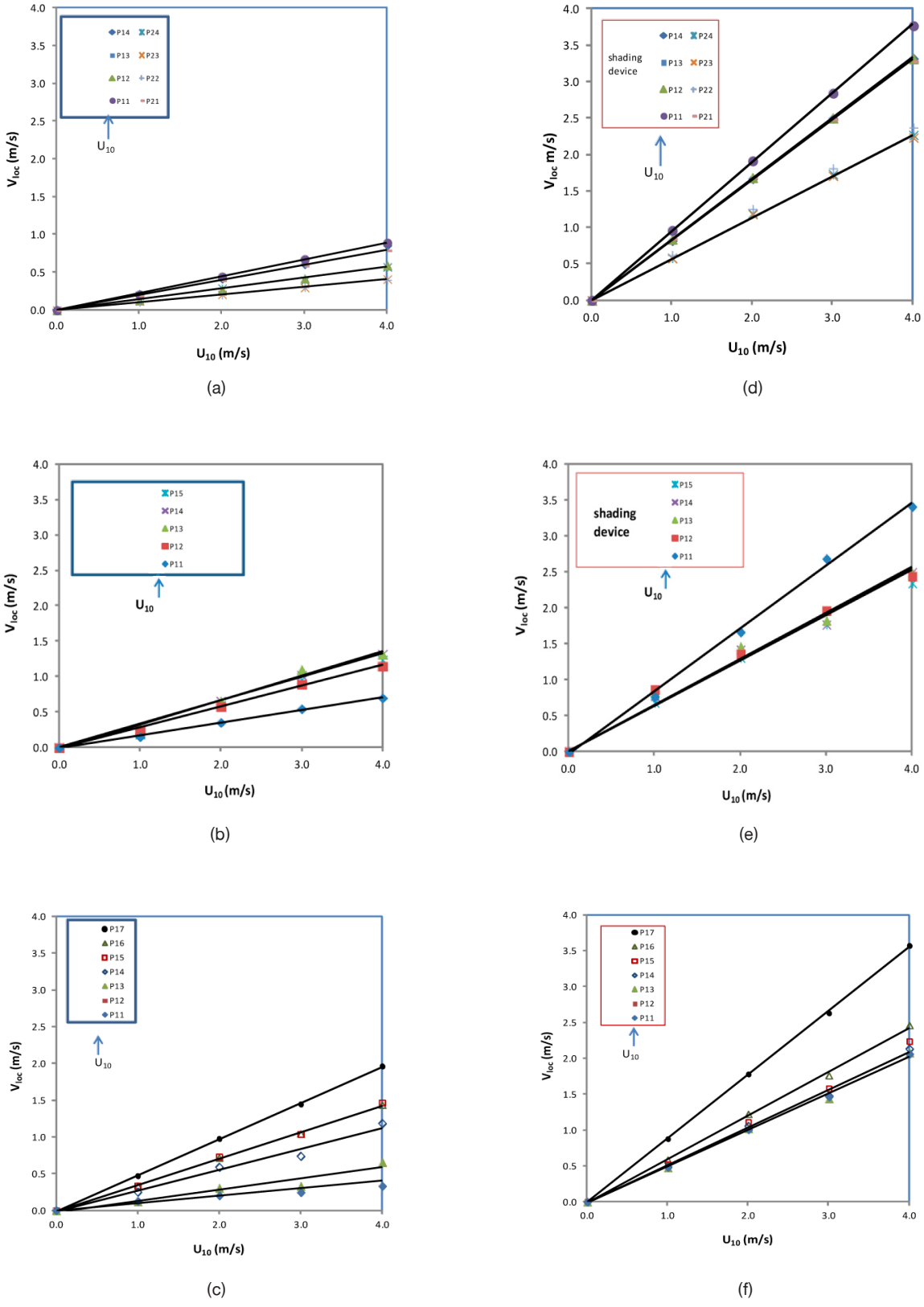

Figure 11. V_{loc} at 0.3 m from the roof (a, b, c) and from the shading device over roof (d, e, f) at points adjacent to center plane.

conveniently practiced in the field so that only the reference wind speed at 10 m (U_{10}) is measured and the local wind velocities (V_{loc}) near the building facade are required. Figure 11a, 11b and 11c shows that the reference wind speed U_{10} of 1.0-4.0 m/s are reduced to 0.4-1.5 m/s in the channel above the roof. The building model #3B with characteristic length of 36 m in the stream wise direction shows high wind velocity at the downstream of the roof due to circulation in that region. In Figure 11d, the local wind velocity over the shading device of the 6 m-high house is highest and almost identical to the reference wind speed because of no disturbance of circulation. In contrast, the circulation above the shading device in Model #3A and #3B reduces the reference wind speed U_{10} from 1.0 m/s to 0.4m/s and from 4.0 m/s to 2.0 m/s at 0.3 m above the surface of the shading device.

4.4.2 *Correlation of h_c Value and V_{loc}*

The power-law correlations between h_c and V_{loc} are found in this study, agreeing with the prediction in previous researches of Loveday & Taki (1996) Blocken et al., (2009) and heat transfer theory. Figure 12, 13 and 14 displays h_c as a function of V_{loc} at 0.3 m above the roof surface and shading device surface. Figure 12-14 can be seen to indicate that a particular value of V_{loc} may give various h_c values depending on the position on the surface. However, the simulation results shows that a reference wind speed (U_{10}) produces various V_{loc} above the roof and above the shading device, varying from 0.0 to 4.0 as depicted in Figure 11. Therefore, Figure 12-14 shall be used as a prediction of h_c value at a point according to the variation of V_{loc} above that point.

Table 2 shows the corresponding correlation of h_c-v_{loc} at selected points on roof and shading device together with their coefficient of determination (R^2). The calculated h_c at v_{loc} = 1 m/s are also provided in Table 2 as examples. The bold characters in Table 2 indicate those points close to the sharp edge of the upstream. Generally, high h_e are found at the upstream point for Model #3A and #3B: however, P11 and P21 of Model #2 are not close enough to detect this sharp acceleration.

From Figure 12, the highest h_c values are found in the center area of the roof and the shading device, i.e. points P12, P13, P22 and P23 of Model #2. At the point near the windward edge such as P11 and P21, both h_e and B_{loc} values are high. The high h_e values above the ceiling of an air conditioned

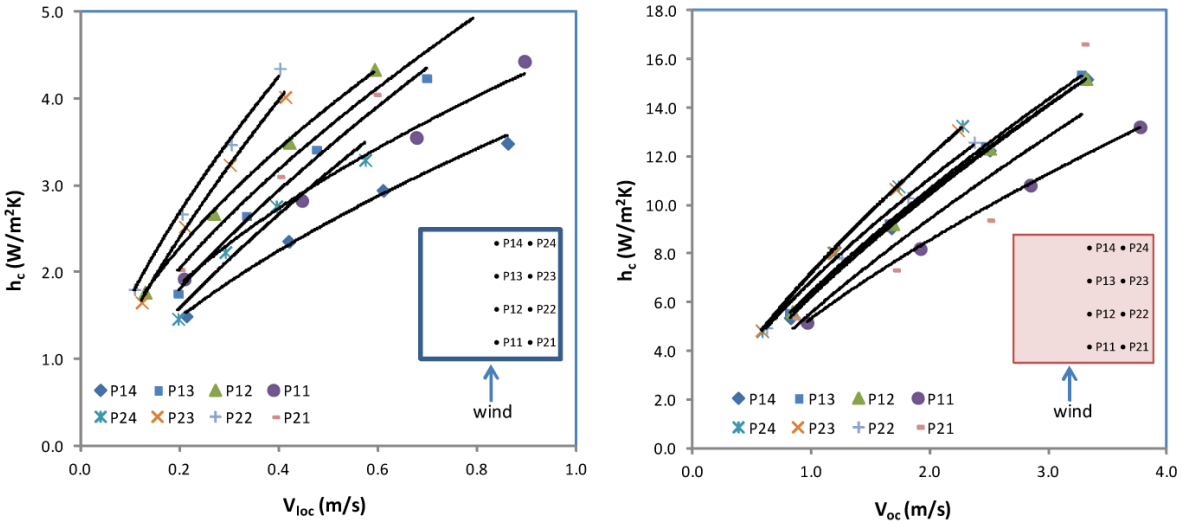

Figure 12. h_c value as a function of V_{loc} for (a) roof and (b) shading device on roof of Model #2.

Table 2. Correlations between h_c and local wind velocity V_{loc} for wind direction normal to the windward edge of the roof and shading device of roof.

Model #	Position	Regression equation (Roof)	R^2	Roof h_c at v_{loc}=1 m/s	Regression equation (Shading device)	R^2
2	P24	$4.56V^{0.56}$	0.992	4.56	$5.34V^{0.68}$	0.999
	P23	$5.86V^{0.59}$	0.999	5.86	$6.40V^{0.72}$	0.999
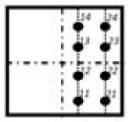	P22	$5.60V^{0.7}$	0.995	5.60	$6.44V^{0.73}$	0.999
	P21	**$3.92V^{0.61}$**	**0.996**	**3.92**	**$6.24V^{0.74}$**	**1.000**
	P14	$5.30V^{0.75}$	0.964	5.30	$7.19V^{0.74}$	0.999
	P13	$7.79V^{0.73}$	0.999	7.79	$7.24V^{0.74}$	0.999
	P12	$7.80V^{0.66}$	0.997	7.80	$6.87V^{0.69}$	0.998
	P11	**$5.72V^{0.64}$**	**0.998**	**5.72**	**$5.58V^{0.76}$**	**0.871**
3A	P45	$2.40V^{0.65}$	0.999	2.40	$7.09V^{0.71}$	0.986
	P44	$2.36V^{0.63}$	0.998	2.36	$7.48V^{0.66}$	0.989
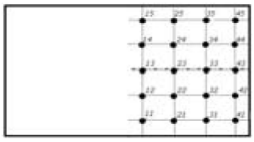	P43	$2.12V^{0.56}$	0.96	2.12	$7.82V^{0.63}$	0.989
	P42	$1.39V^{0.19}$	0.791	1.39	$8.11V^{0.57}$	0.985
	P41	**$5.28V^{0.69}$**	**0.999**	**5.28**	**$6.86V^{0.69}$**	**0.983**
	P35	$2.25V^{0.56}$	0.820	2.25	$10.84V^{0.63}$	0.990
	P34	$2.21V^{0.49}$	0.878	2.21	$11.37V^{0.52}$	0.992
	P33	$1.91V^{0.53}$	0.986	1.91	$11.79V^{0.44}$	0.986
	P32	$1.42V^{0.27}$	0.713	1.42	$12.92V^{0.53}$	0.995
	P31	**$4.73V^{0.64}$**	**0.996**	**4.73**	**$9.15V^{0.56}$**	**0.987**
	P25	$1.94V^{0.51}$	0.978	1.94	$17.18V^{0.81}$	0.957
	P24	$1.89V^{0.49}$	0.973	1.89	$21.83V^{0.79}$	0.944
	P23	$1.70V^{0.40}$	0.905	1.70	$27.29V^{0.87}$	0.762
	P22	$1.35V^{0.17}$	0.536	1.35	$25.99V^{1.03}$	0.937
	P21	**$4.62V^{0.60}$**	**0.992**	**4.62**	**$10.03V^{0.58}$**	**0.987**
	P15	0.83V+1.07	0.844	1.90	-	-
	P14	0.69V+1.14	0.75	1.83	-	-
	P13	-		-	-	-
	P12	-		-	-	-
	P11	**$4.50V^{0.57}$**	**0.985**	4.50	**$10.54V^{0.53}$**	**0.988**
3B	P27	-	-	-	$1.88V^{0.69}$	0.999
	P26	$1.74V^{0.44}$	0.948	1.74	$2.12V^{0.69}$	0.998
	P25	$2.07V^{0.64}$	0.998	2.07	$2.20V^{0.69}$	0.998
	P24	$2.13V^{0.59}$	0.992	2.13	$2.19V^{0.68}$	0.999
	P23	$2.40V^{0.51}$	0.916	2.40	$2.10V^{0.67}$	0.997
	P22	$2.86V^{0.57}$	0.975	2.86	$2.06V^{0.68}$	0.995
	P21	**$2.70V^{0.55}$**	**0.998**	**2.70**	**$2.02V^{0.55}$**	**0.941**
	P17	-	-	-	$1.56V^{0.65}$	0.961
	P16	$1.44V^{0.30}$	0.735	1.44	$1.76V^{0.70}$	0.998
	P15	$1.81V^{0.53}$	0.976	1.81	$1.95V^{0.68}$	0.997
	P14	$1.76V^{0.38}$	0.794	1.76	$2.07V^{0.68}$	0.998
	P13	-	-	-	$2.07V^{0.68}$	0.998
	P12	$2.47V^{0.39}$	0.772	2.47	$2.02V^{0.65}$	0.995
	P11	**$3.56V^{0.61}$**	**0.899**	**3.56**	-	-

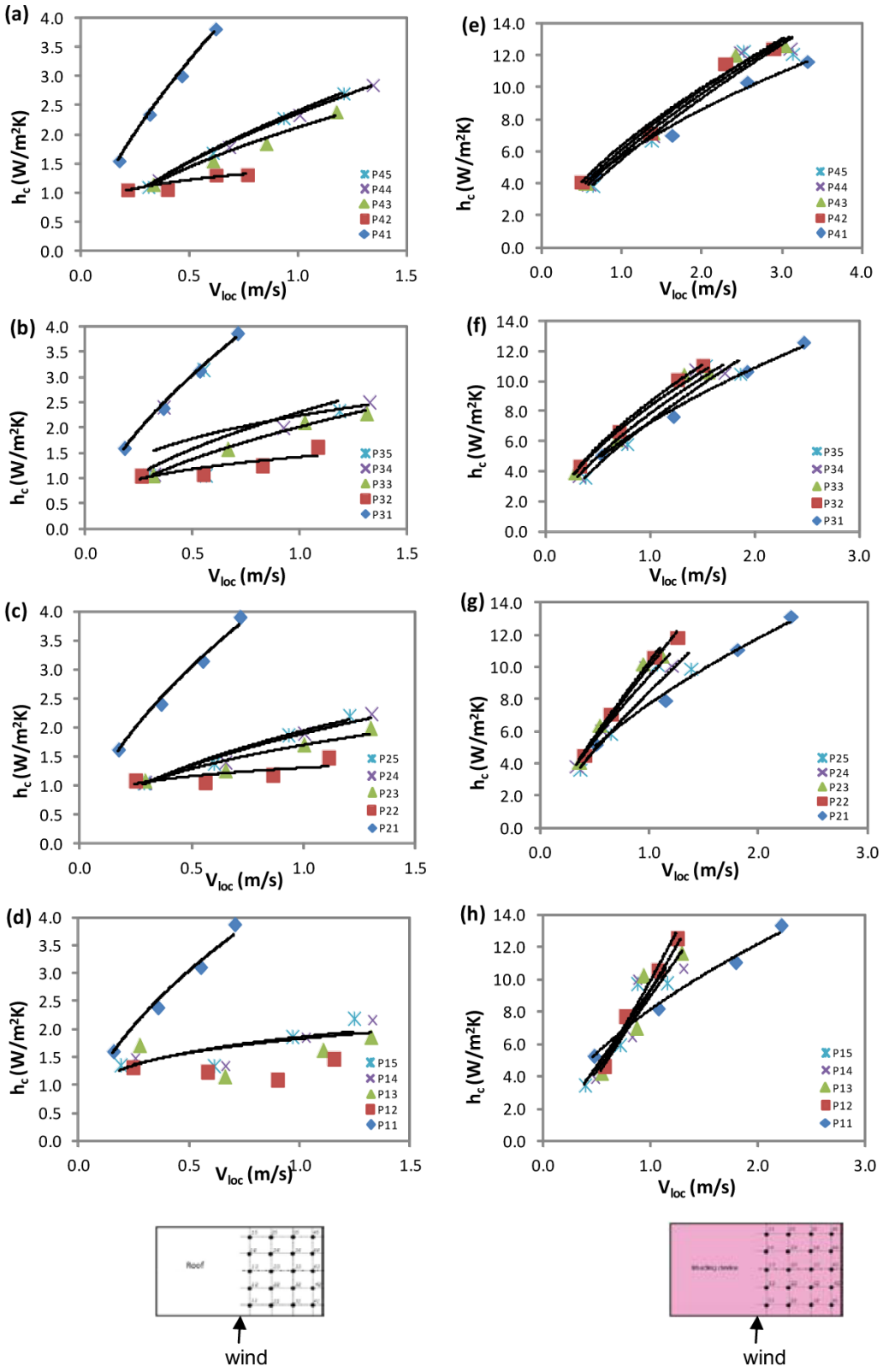

Figure 13. The h_c value as a function of V_{loc} for roof (a, b, c, d) and shading device on roof (e, f, g, h) of Model #3A.

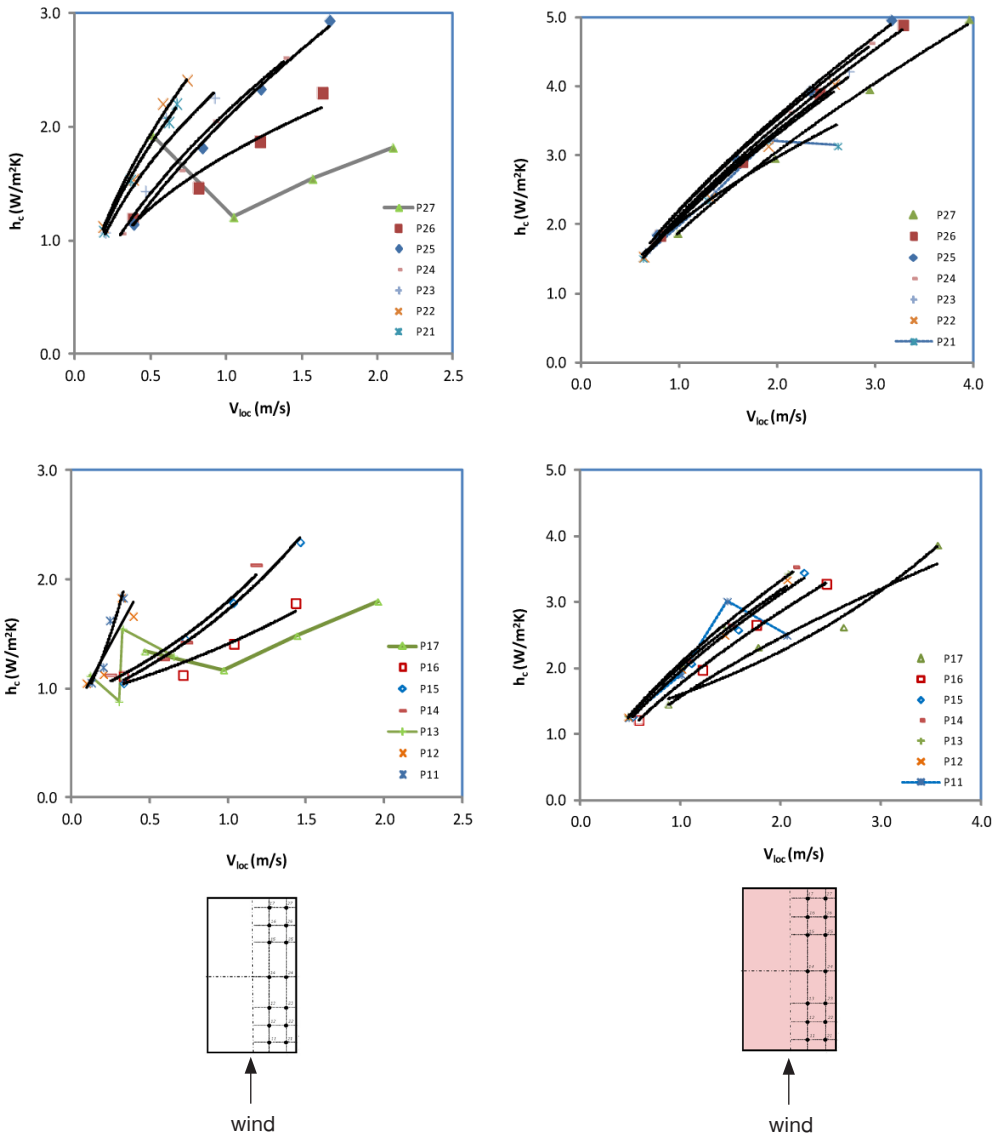

Figure 14. h_c value as a function of V_{loc} for (a) roof and (b) shading device on roof of Model #3B.

room could bring large heat and moisture transfer from the external surface into the room. Simulation results of a two storey house suggest that an energy efficient room should avoid being placed in the windward edge and the middle of the floor plan. On the other hand, if ambient temperature is lower than that of the building surface, high h_c values are required to reduce heat absorption in the roof.

There are some points of Model #3A with high fluctuation of h_c regarding V_{loc} such as points P12, P13, P14 and P15 on the roof and its shading device. With an increase in the V_{loc} above the roof and shading device, h_c values do not change with the power law as shown in Figure 13(d) and 13(h). Distribution of h_c in Model #3A is different from those of the Model #2. The low h_c are found in the center of the surface such as points P22, P23, P32, and P33.

Shown in Figure 14, the h_c values at points P11, P13, P17 and P27 of the roof and shading device of Model #3B also oscillate depending on the V_{loc}. Hence the regression functions as power law of these points are not shown in Table 2. For other points, the power law captures the distribution of h_c values effectively with high correlation R^2. The low h_c values in Model #3B are found in the center and leeward of the surface such as points P14, P15, and P16.

5. Conclusions and Recommendations

Medium-resolution 3D transient LES CFD simulations of forced convective heat transfer at the roof and shading device of the roof of a low-rise building are performed to determine convective heat transfer coefficient (h_c). The low-rise building models have dimensions of 8 x 8 x 6 m^3, 36 x 20 x 14 m^3 and 20 x 36 x 14 m^3, representing a 2-storey house, a 4-storey row building with 36 m in the wind direction, and a 4-storey row building with 20 m in the wind direction, respectively. It should be noted that this study investigates only the wind direction normal to the edge of the roof. The following conclusions are made:

1) The CFD validation based on an experimental small scale cube model has shown that the constructed cube model (Model #1) with transient LES approach of standard SMG can provide an acceptably accurate result for convective heat transfer distribution over the top surface of the cube.

2) The local wind velocity at 0.3 m above the surfaces (V_{loc}) is explored at points on the surfaces and found as linear functions of reference wind speed (U_{10}). The values of U10 are reduced from 1.0-4.0 m/s to 0.4-1.5 m/s for every point on the roof and shading device surfaces.

3) This study confirms the power-law function between h_c values and V_{loc}. The coefficients of determination (R^2) of most of points are high ($\cong$1.000). There are oscillation of this function especially for points in the channel between the roof and the shading device. Further study of small time-step simulations with high resolution is recommended.

4) The three building models show high h_c values at the sharp upstream edge and at the two edges of side walls. At the center areas of the roof and the shading device, low h_c values are found in the 4-storey buildings but high h_c values are found in the 2-storey house. Therefore, the highest convective heat transfer to or from the 4-storey building's roof are on the upstream edges. For a house, high heat transfer occurs almost all over the area, except at the downstream edge. Comparing the three building models, the 2-storey house shows the highest values of h_c and the 4-storey building with 36 m in the wind direction shows the smallest values of h_c. A large area of h_c value of 0.8-1.5 W/m^2K is found from the center area towards the downstream edge of this building.

5) From the simulation results, a 4-storey building could be sensitive to heat and moisture transfer at its edges. Building designers may consider installing long eaves at the top floor or using buffer zones around the building core especially for the top floor. Simulation results of a 2-storey house show a high convective coefficient for most of the top surface. Though the shading device is presented for heat protection, preventing heat and moisture flowing into top-floor room would be difficult in the case of a 2-storey house.

References

Blocken, B., Defraeye, T., Derome, D. & Carmeliet, J. (2009). High-resolution CFD simulations for forced convective heat transfer coefficients at the facade of a low-rise building. *Building and Environment,* 44, 2396–2412.

Concentration Heat and Momentum Limited [CHAM]. (2010). *PHOENICS Documentation: TR 000*. Retrieved April 18, 2012, from http://www.cham.co.uk/ChmSupport/tr000.php

Cheng, Y., Lien, F. S., Yee, E. & Sinclair, R. (2003). A comparison of large Eddy simulations with a standard k–e Reynolds-averaged Navier–Stokes model for the prediction of a fully developed turbulent flow over a matrix of cubes. *Journal of Wind Engineering and Industrial Aerodynamics*, 91, 1301–1328.

Chungloo, S. (2007). *Experimental and numerical studies of solar chimney and wetted roof: An application in the hot and humid climate.* Ph.D. Thesis. Sirindhorn International Institute of Technology, Thammasat University, Kingdom of Thailand.

Givoni, B. (1994). *Passive and low energy cooling of buildings.* Wiley, New York.

Hagishima, A. & Tanimoto, J. (2003). Field measurements for estimating the convective heat transfer coefficient at building surfaces. *Building and Environment,* 38, 873–881.

Hemida, H., Spehr, F., Krajnovic, S. (2008). Local heat transfer enhancement around a matrix of wall-mounted cubes using passive flow control: Large-eddy simulations. *International Journal of Heat and Fluid Flow,* 29, 1258-1267.

Loveday, D. L. & Taki, A. H. (1996). Convective heat transfer coefficients at a plane surface on a full-scale building facade. *Int. J. Heat Mass Transfer, 39*(8), 1729-42.

Meinders, E. R., Van der Meer, T. H. & Hanjali, K. (1998). Local convective heat transfer from an array of wall-mounted cubes. *International Journal of Heat and Fluid Flow,* 41, 335-346.

Meinders, E. R. & Hanjali, K. (1999). Vortex structure and heat transfer in turbulent Flow over a wall-mounted matrix of cubes. *International Journal of Heat and Fluid Flow,* 20, 255-267.

Rodi, W. (1997). Comparison of LES and RANS calculation of the flow around bluff bodies. *Journal of Wind Engineering and Industrial Aerodynamics,* 69, 55-75.

Versteeg, H. K. & Malalasekra, W. (1995). *An Introduction to Computational Fluid Dynamics: The Finite Volume Method.* UK: Longman Scientific & Technical.